Design of a Charge-Breeder Ion Source for Texas A&M University[*]

Wayne D. Cornelius, Scientific Solutions, San Diego CA USA[†]

Abstract

Scientific Solutions designed and fabricated a 14.5 GHz charge-breeder ECR source for the Texas A&M University Cyclotron facility. This charge-breeder source was designed as a charge-breeder from the start rather than as a conversion of an existing ECR system. In addition, the overall system was designed to be modular so that various components can be easily substituted to facilitate technology developments. This paper details the overall design, the design constraints, and reviews specific performance requirements that resulted in this particular system design.

BACKGROUND

The purpose of this project was to provide a test bed for developing technology and techniques specific to charge-breeder electron-cyclotron resonance (ECR) ion sources. Unlike "primary" ECR sources where the unionized elemental feedstock is introduced into the source as neutral atoms, a charge-breeder is designed for injection of short-lived radioactive ions. Because these exotic ions are produced in nuclear reactions, the number of ions is always severely limited. Therefore the overall efficiency of the charge-breeder source is extremely important. The source efficiency is the product of the injection efficiency, the ionization efficiency, the ion extraction efficiency, and the effective dwell time in the source. This project not only created a charge-breeder system for producing the highly charged ion species needed for nuclear physics experiments, but one that could be used as a test bed for testing and developing additional techniques and technologies.

DESIGN RULES

Once the choice of operating frequency is made, the design of the magnetic circuit is the next most important feature. The optimal magnetic field profile of a high charge-state ECR ionizer was determined primarily through trial-and-error over the last ten to fifteen years. [1-4] The preferred field profile has a peak magnetic field at the beam extraction point approximately equal to twice the ECR resonant field, B_{ECR}, (~2.79 GHz/kGauss). The minimum magnetic field should be in the range of $0.8 \cdot B_{ECR}$.[5] The peak magnetic field at the end opposite extraction has been the subject of more discussion.[6] Some argue that $2 \cdot B_{ECR}$ is adequate while others claim improved performance with fields up to $5 \cdot B_{ECR}$. Such high fields are generally obtained by inserting steel plugs into the bore of the solenoid magnet. However it is not possible to reach $3 \cdot B_{ECR}$ or higher without blocking a substantial part of the bore of a conventional copper-coil solenoid magnet. Blocking the bore blocks injection of ions. This conflict represents a major incompatibility between charge-breeders and primary ECR sources.

The bore of the solenoid is the next most important parameter in the overall system design (after the magnetic field profile). The bore should be as large as possible to maximize the diameter of the plasma chamber. However the sextupole magnet surrounding the plasma chamber pushes this critical dimension to values larger than can be excited by room-temperature copper coils when the ID of the plasma chamber exceeds 9 cm. As discussed below, 8" (20 cm) is the largest bore compatible with 14.5 GHz operation, a strong sextupole magnet, and copper coils.

The sextupole magnet plays an extremely important role in the confinement and stabilization of the plasma. To minimize electron loss to the interior walls of the plasma chamber, the sextupole should have a field magnitude of at least $2 \cdot B_{ECR}$ at the interior surface.

We chose a 24-block Halbach ring configuration [7] because this design makes the most efficient use of expensive permanent magnet material and provides the highest magnetic field strength available per unit mass of magnet block. The Halbach configuration rotates the magnetization vector at three times the rotation angle around the cylinder. This rotation effectively cancels the magnetic field outside the cylinder while doubling the interior field strength. The peak field at the inner wall of the plasma chamber of $2.2 \cdot B_{ECR}$. This radial field is significantly stronger than most primary ECR sources and is expected to significantly improve the performance.

Note that the cylindrical Halbach array completely surrounds the plasma chamber and permits no radial access. However a charge-breeder system should not require peripheral components, such as ovens or sample insertion ports. Therefore not having radial access should not be a disadvantage.

The ion injection system is comprised of a pair of electrostatic lenses and the beam extraction system is a relatively conventional "puller" assembly with an added electron trap to prevent electrons from backstreaming into the ion source.

DESIGN FEATURES

This charge-breeder design has a number of features that facilitate maintenance and repair, protect critical components, promote long operational lifetime, and enable technology development. These features include 1) no water-to-vacuum joints, 2) cooling channels between the plasma "cusps" and the sextupole magnet, 3) ample vacuum pumping of interior rf waveguides, 4) modular design with replaceable components, 5) mounting of solenoids and charge-breeder system on ball-bushing rails.

Charge Breeding

SOLENOID MAGNETS

We used the design of the AECR-U solenoid magnets[1] as a starting point for our solenoid design study. These solenoids have demonstrated good performance and have operated reliably for a number of years. During this design study it became clear just how well matched the AECR-U solenoids are to the ECR requirements.

We were unable to increase the bore of these magnets without exceeding current density and steel saturation limits. The steel endwalls of the AECR-U shell are thick enough to keep most of the steel below saturation. However the steel plug is badly saturated with internal fields approaching 32 kGauss. This saturation contributes to a decrease in the efficiency of the excitation coils, requiring more excitation current. Increasing the solenoid bore increases the flux density in the steel plug and exacerbates the coil design problem. These effects resulted in our choice to limit the bore to 8" (20 cm).

A section view of the final solenoid configuration is shown in figure 1. The bore limits the maximum magnetic field to about $2.5 \cdot B_{ECR}$. However, as noted above, this system was designed to facilitate replacement of components. The steel plug could be replaced by one with a smaller bore if the electrostatic injector is replaced with a sextupole ion guide (SPIG).

Figures 2a and 2b compare the measured magnetic fields of the individual solenoids with the theoretical curves and 100 A excitation current. Figure 3 compares the measured field of both solenoids with 50 A excitation current in their final charge-breeder configuration. Although the solenoids were designed to operate with up to 500 Amps of excitation current, The facilities in San Diego limited the power to 2 kW of cooling. Hence the solenoids could be tested up to a maximum of 100 Amps in one solenoid or 50 Amps in two.

Solenoid #1 showed excellent agreement with the predicted magnetic field profile (figure 2a). Initially however, the magnetic field of solenoid #2 was somewhat weaker than expected (open red squares in figure 2b). Further investigation showed that one of the coils was shorted between the lead-in conductors outside the steel shell. Installation of a mylar sheet between the lead-in conductors removed the short and the field profile was exactly as predicted (blue dots in figure 2b). As a result of this discovery, mylar insulation was installed between all of the coil leads to eliminate the potential for shorted coils.

SEXTUPOLE MAGNET

The sextupole magnet is a Halbach array of keystone blocks arranged in a series of six rings with 24 blocks per ring (figure 4). The Halbach configuration results in near cancellation of the magnetic field outside the ring and a near doubling the field strength inside the ring. The magnetic field just inside the inner wall of the plasma chamber is 1.14 Tesla (e.g. $\sim 2.2 \cdot B_{ECR}$). This strong sextupole field provides much improved radial

confinement of the plasma compared with the multiple bar arrays typical of primary ECR sources. Note however that the Halbach configuration precludes radial access to the plasma chamber. While this lack of radial access might be a problem with primary ECR sources, it is not expected to be a problem in a charge-breeder because the beam ions are axially injected.
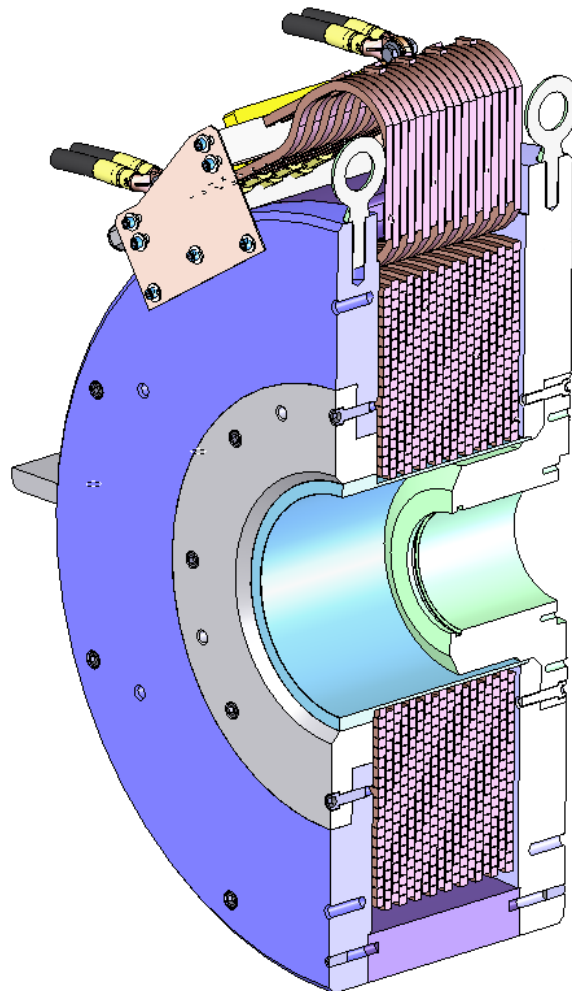

Figure 1. Section view of charge-breeder solenoid.

QA measurements were performed on the sextupole magnet to ensure that all magnet blocks in the assembly were of uniform strength and were oriented correctly so that the magnetic field profile had no significant weak areas that could reduce the plasma confinement efficiency. These measurements were made using a rotating wire loop. The rotation angle was derived from a shaft encoder with 540 steps per 360° rotation. Analysis of the resulting sine wave was used to derive the field components as a function of distance down the bore of the cylinder (figure 5).

The loop voltages showed a consistent pattern of 49 and 51 Hz signals that were coming from an uninterruptable power supply in the neighboring suite. We were unable to completely eliminate these spurious signals. However the

Charge Breeding

results of these measurements were not particularly sensitive to these relatively high frequency signals. The error bars shown in figure 5 include the effects of the spurious signals.
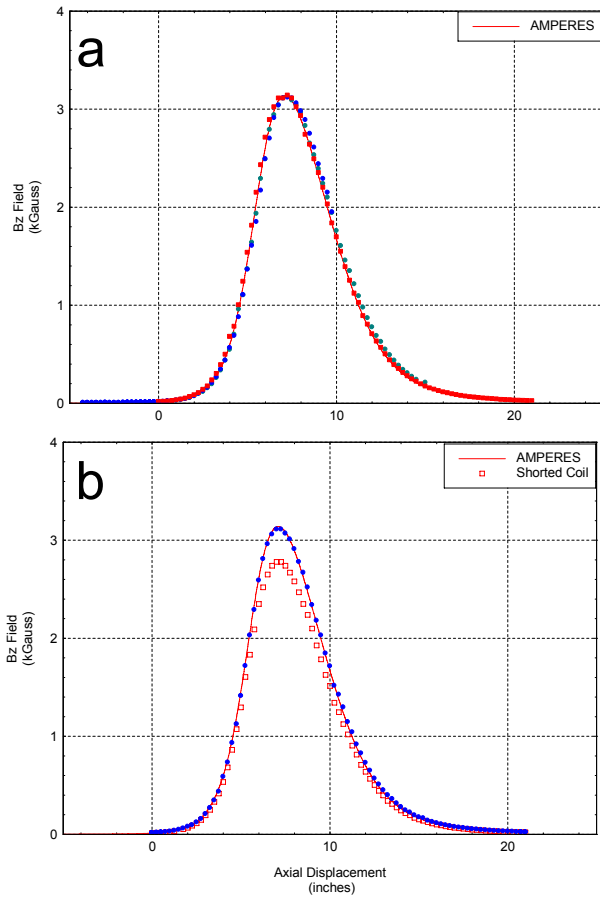

Figure 2. Comparison of the measured magnetic field profile of solenoid #1 (a) and solenoid #2 (b) with the theoretical field profile (red curve) for 100 A excitation current.
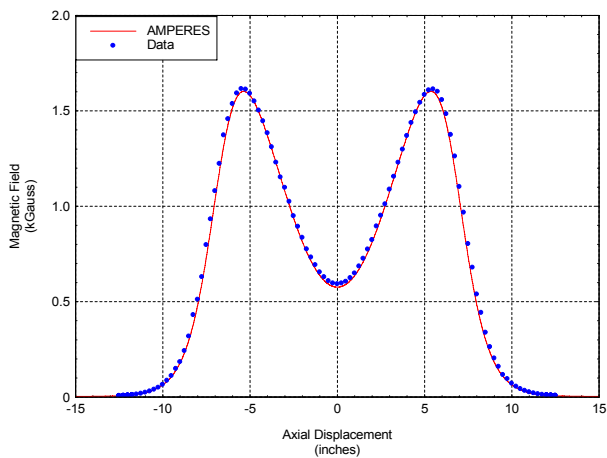

Figure 3. Comparison of the measured magnetic field profile of the charge-breeder solenoids (blue dots) with

the theoretical profile (red line) for 50 A of excitation current.

Figure 4. View of partially assembled Halbach sextupole magnet showing the individual magnet blocks.

The data were analyzed using two different methods. The first method fit the waveform with a sine wave and the second computed the FFT of the waveform. The results of both analyses are shown in figure 5. The solid black rectangle indicates the outline of the sextupole magnet. The blue dots plot the magnitude of a sine-wave fit to the data (left-hand axis) and the red squares plot the FFT magnitude (right-hand axis). Note that, except for end effects, these data show relatively uniform field magnitude in the sextupole magnet. Typical accelerator beam applications require quantification of the non-sextupole components of the field. However the non-sextupole components have little effect on the confinement of the plasma and were not derived from the rotating-loop data.
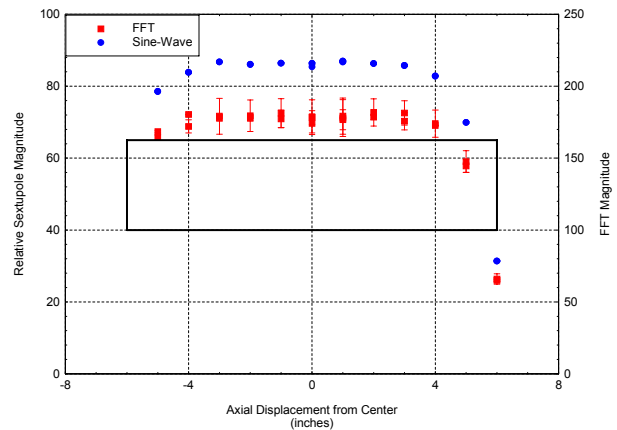

Figure 5. Results from the QA testing of the sextupole magnet. The blue dots plot results from fitting the

Charge Breeding

waveforms with a sine wave and the red squares plot the FFT magnitude of the waveforms.

The bore and both ends of the sextupole assembly are sealed with 0.025" thick stainless steel. Hence the sextupole is completely encapsulated in a corrosion-resistant shell. This approach allows cooling water to flow in the space between the plasma chamber and the inside of the sextupole shell without wetting the permanent magnet material. Getting cooling into this region is critical. Virtually all ECR sources have damaged their sextupole magnets at one time or another. Our design has "flats" onto the outside of the plasma chamber so that the cooling water can flow between the OD of the plasma chamber and the ID of the sextupole and intercept the heat between its source (the inside wall of the plasma chamber) and the magnet blocks (figure 6). This approach protects the expensive sextupole magnet from the plasma.
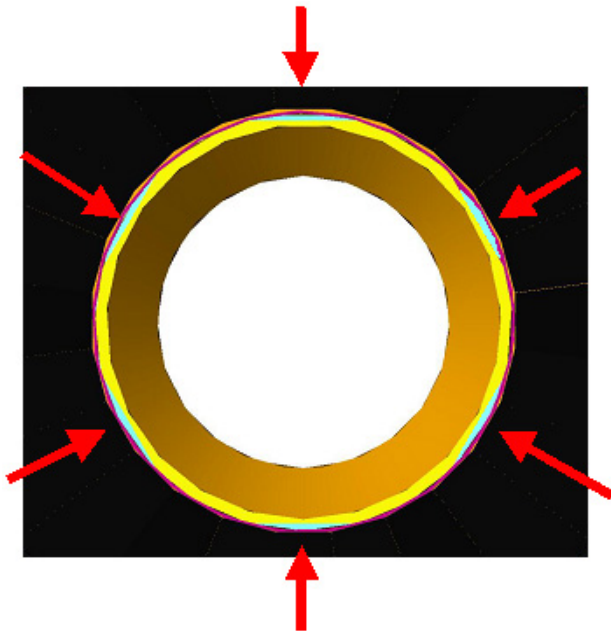

Figure 6. Sectioned view of the sextupole magnet assembly surrounding the plasma chamber. The cooling water (cyan) flows in the space between the "flats" on the OD of the plasma chamber and the ID of the sextupole assembly (red arrows).

PLASMA CHAMBER

A major design goal of this project was to provide flexibility so that the charge-breeder system could be used as a test bed to develop other techniques and technologies. Hence the plasma chamber was designed to be a very simple system that can be easily replaced.

The plasma chamber is made from thick-walled 6061 aluminum tube. The interior of this tube is bored out to produce a 9 cm ID chamber. Six "flats" were cut into the OD of the tube on the periphery of the plasma region (figure 6). As discussed above, cooling water flows in the region between these flats and the ID of the sextupole magnet. The minimum thickness of aluminum in the

center of each flat is 1 mm. The pressure differential between the vacuum and the cooling water stresses this region. Stress analysis of the plasma chamber indicates a safety factor of 4.8 times the yield stress.

HIGH VOLTAGE ASSEMBLY

Figure 7 is a section view of the high voltage assembly including the plasma chamber (gold), high voltage insulators (white), and sextupole magnet (cyan shell surrounding the gray magnet blocks). The plasma electrode (also called extraction electrode or beam-formation electrode) is not shown, but mounts to the flange on the ID of the plasma chamber (right-hand end). The injection endwall seats against the ridge on the ID of the plasma tube (left-hand end). The vacuum is sealed by o-rings at each end of the plasma chamber. These circumferential o-rings help to align the plasma chamber with the axis of the solenoids and do not require fasteners to compress them. The cooling water pressure is sealed by a pair of o-rings on the outside surface of the plasma chamber in a separate location. Hence there are no water-to-vacuum o-ring joints in this assembly.

The plasma chamber and sextupole assembly are isolated from ground by a pair of Rexolite [8] insulators (red arrows in figure 7).
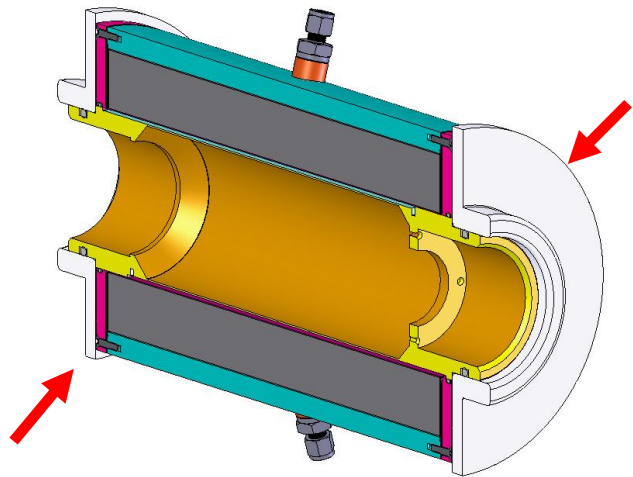

Figure 7. Section view of the high voltage assembly (plasma chamber, sextupole magnet, and high voltage insulators). The HV insulators are indicated by the red arrows.

Figure 8 shows the completed high voltage assembly ready for installation into the solenoid magnets. One of the Rexolite insulators is shown on the near end in the figure. The other is already mounted in the solenoid plug. The vacuum seal is made by o-rings on the ID of the steel solenoid plugs.

One of the solenoid magnets is mounted on rails to facilitate installation of the high voltage assembly. The solenoids are separated by turning a hand crank and the high voltage assembly is inserted between the two

magnets as shown in figure 10. The precision rails ensure that the alignment of the solenoids is preserved during the installation process. Once the high voltage assembly is installed, the separation of the solenoids is reduced by turning the crank. The hand crank provides the "feel" needed to ensure the o-rings are properly seating against the Rexolite. The final separation of the solenoids is locked with three turnbuckle assemblies connecting the inside steel endwalls of the solenoids.
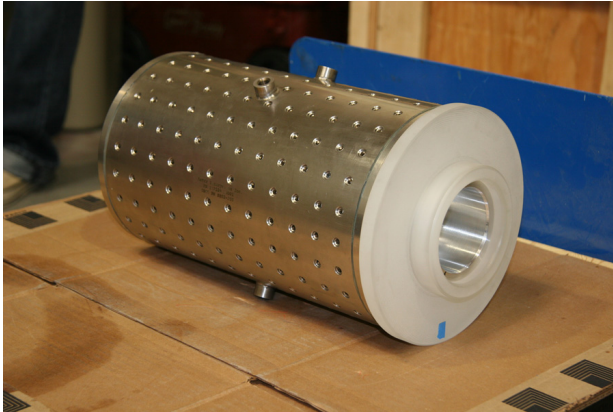

Figure 8. High voltage assembly ready for installation in the solenoid magnets.

Figure 9. Installation of the high voltage assembly in the charge-breeder solenoids.

BEAM EXTRACTOR

Figure 10 is an isometric section view of the extractor end of the charge-breeder. The extractor is a relatively conventional puller assembly with two electrodes attached to the cylindrical ground shield. The first electrode is biased negative with respect to ground to prevent electrons produced by ionization of the residual gas from being accelerated backwards into the ion source. These electrons can cause a variety of operational problems from overloading the high voltage power supply to burning through metal surfaces inside the source.

Note how the extractor assembly can be easily exchanged, substituted, or modified by attaching an alternative assembly to the mounting flange (blue) or by replacing the mounting flange. Additional space is available within the vacuum cross for mounting

Charge Breeding

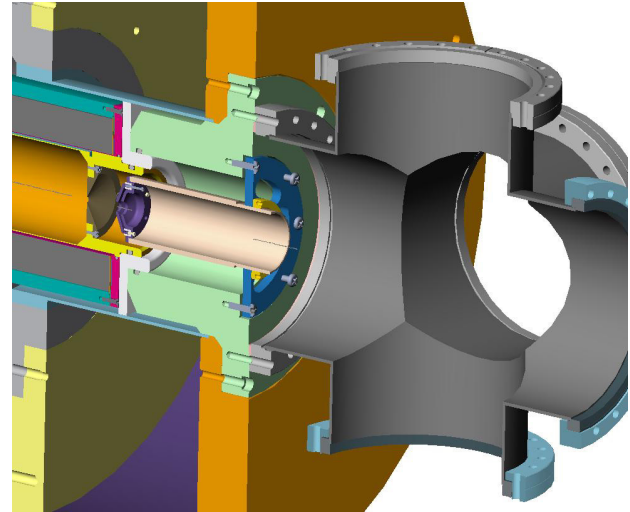electrostatic lenses, steering magnets, or diagnostic devices.

Figure 10. Isometric cross section of the extractor end of the charge-breeder showing the relative locations of the plasma chamber (gold), the plasma aperture (brown), the puller electrodes (violet), the puller mounting flange (blue), a Rexolite insulator (white), the steel solenoid end plug (blue-green), and the vacuum cross (gray). The solenoid coils are not shown.

Figure 11 details the area of the extraction gap. Note the two electrodes on the puller assembly (violet) and their location with respect to the plasma aperture (brown). Note also the vacuum o-rings on the ID and OD of the white Rexolite high voltage insulator and the smaller o-ring on the ID of the magenta sextupole flange. The small o-ring confines the cooling water to the ID of the sextupole magnet so that we have no water-to-vacuum o-ring joints. The extractor assembly is shown in figure 12.
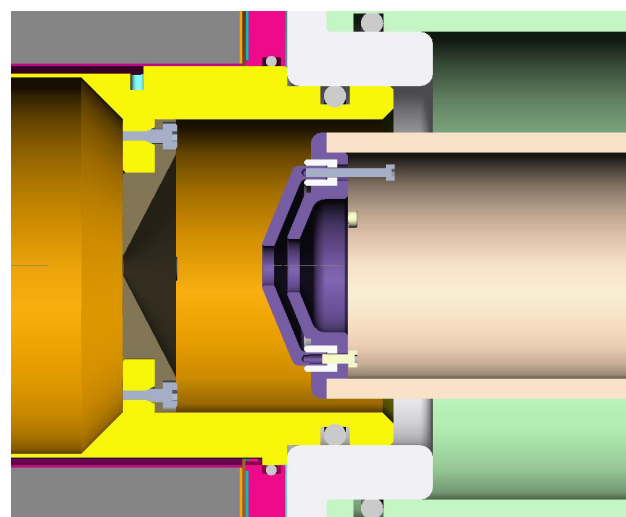

Figure 11. Detail cross section of the extractor end of the charge-breeder showing the relative locations of the plasma chamber (gold), the plasma aperture (brown), the puller electrodes (violet), the Rexolite insulator (white), and the steel solenoid end plug (blue-green)

Figure 12. Extractor assembly of the charge-breeder source. The puller electrode is isolated from ground by the white Macor insulator and can be biased up to –2 kV with respect to ground.

BEAM INJECTOR

The injector is one of the more critical components of the charge-breeder system. The final energy of the injected ions needs to be no more than a few eV if these ions are to be effectively stripped of more electrons in the plasma. Too high an energy and the ions pass through the charge-breeder without interacting with the plasma. Too low an energy and the ions are repelled by the floating potential of the plasma chamber. Because the parameters of the effective source of ions (i.e. the helium gas cell) are not yet well characterized, we made the assumption that the emittance of the injected beam would be relatively poor. A design capable of injecting a poor emittance beam should be capable of transporting higher quality emittance beam.

Figure 13 shows results of simulated injection of 10 keV ^{84}Kr$^+$ ions for a variety of Einzel lens voltages. Each grid square represents 1 cm in radial and longitudinal displacement. The ion trajectories are denoted by the lines originating at the left and continuing to the right. The Einzel lens electrode is denoted by the gray bar at the top of the frame approximately one-third of the way from the left-hand side. A grounded metallic shield is denoted by the horizontal, angled, and horizontal gray shape denoted with 0V. The plasma chamber endwall and bias disk are represented by the gray rectangles at the right-hand end.

Increasing the voltage on the Einzel lens focuses the ions towards the injection aperture. Note however that when the beam ions no longer intercept the ground shield (~7.0 kV), the ions still intercept the plasma endwall. This effect demonstrates that the distance between the Einzel lens and the endwall aperture is too large. Additional aberrations are due to the magnetic field.

These aberrations can be seen by noting how the increasing voltage on the Einzel lens "rolls over" the

outside ion trajectories rather than smoothly focusing ions at all radii. These focusing aberrations result from the combination of electric and magnetic fields. Electrostatic focusing of the beam induces a velocity component transverse to the magnetic field. As a result, the beam ions begin to rotate around the flux lines. This rotation reduces the effectiveness of the electrostatic focusing and leads to the aberration evident in figure 13.
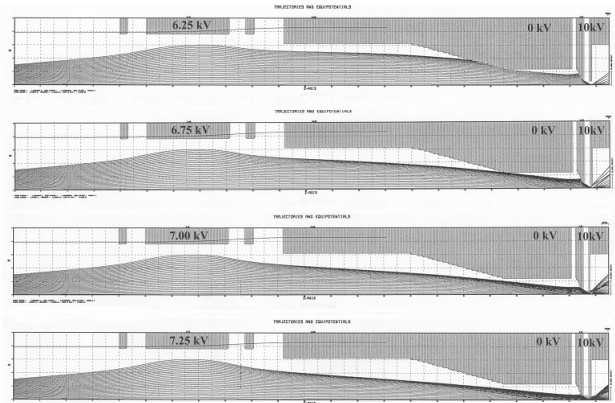

Figure 13. Injected ion trajectories for voltages of 6.25, 6.75, 7.00, and 7.25 kV on the Einzel lens.

Figure 13 demonstrates the need for a second Einzel lens near the injection aperture. An additional benefit of this approach is a reduction in the voltage difference between the injection endwall (at +10 kV) and the second Einzel lens (+2 to +6 kV). Reducing this voltage difference reduces the magnitude of the electric field at the plasma aperture and reduces the ion current extracted from the wrong end of the charge-breeder.

Figure 14 compares ^{84}Kr$^+$ ion injection with 6.75 kV on the first Einzel lens and a variety of voltages on the second Einzel lens (top to bottom 0, 1, 2, 3, 4, and 5 kV). Note how increasing the voltage on the second Einzel lens improves the injection efficiency. In the last case (5 kV), magnetic focusing of the outside trajectories begins to dump beam ions on the injection aperture (similar to the bottom view in Figure 13). Figure 14 indicates a comfortable range of Einzel lens voltages that result in acceptable ion injection compared with the single lens design in figure 13. The charge-breeder injection scheme utilizes a pair of cylindrical electrostatic lenses to focus the ion beam into the plasma chamber.

Figure 15 shows the first Einzel lens and ground shield of the injector assembly. These components are attached directly to a mounting flange in a manner similar to the extractor electrodes. The ground shield protects the ion beam from the voltages on the components attached to the plasma chamber. Without this shield, the electric fields could disrupt the beam ions by steering and shearing the injected beam. The ground shield is electrically isolated from ground so that ion current impinging on the shield can be measured as a diagnostic tool. The mounting flange has the same pusher/puller alignment screws as the extractor assembly.
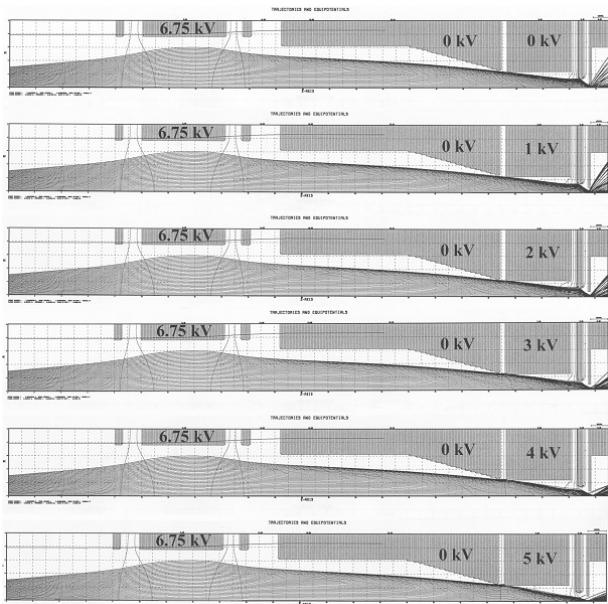
Figure 14. Comparison of $^{84}Kr^+$ ion trajectories for a variety of secondary Einzel lens voltages (from top to bottom: 0, 1, 2, 3, 4, and 5 kV).

Figure 15 details the charge-breeder injection system. The components include the WR-75 waveguide, ground shield, two Einzel lenses, plasma chamber endwall. Also shown are the sextupole magnet, Rexolite high voltage insulator, solenoid end plug, and the vacuum cross. The solenoid coils are not shown. Figure 16 details the region around the plasma chamber endwall.
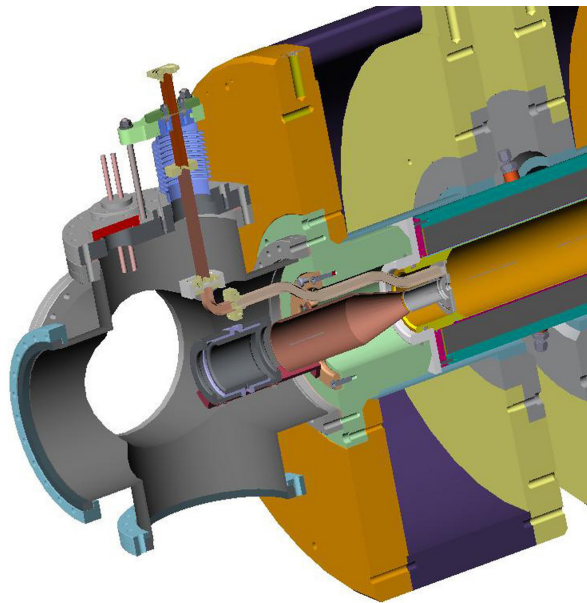

Figure 15. Section view detailing the injection end of the charge-breeder. The solenoid coils are not shown.

Figure 17 shows the plasma endwall sub-assembly. Included in this sub-assembly are the plasma chamber endwall, the WR-75 waveguide, the second Einzel lens, and the gas feed tube. Figure 18 is a close-up of the exterior of the endwall assembly. The second Einzel lens

(cylinder) is isolated from the endwall by two ceramic insulators (white). The plasma endwall is water-cooled via the two copper cooling tubes attached to the waveguide and to the plasma endwall. These tubes pass through o-ring seals to the outside so that the system has no water-to-vacuum joints. The wire coming out of the near side in figure 18 (blue arrow) is for connecting the voltage to the bias disk on the inside of the endwall. The gas feed tube can be seen below the cylindrical Einzel lens. The rf spring-ring on the outside diameter of the endwall ensures good electrical contact with the interior surface of the plasma chamber. The slots in the waveguide allow gas atoms to escape from the interior and ensure good vacuum pressure inside the waveguide.
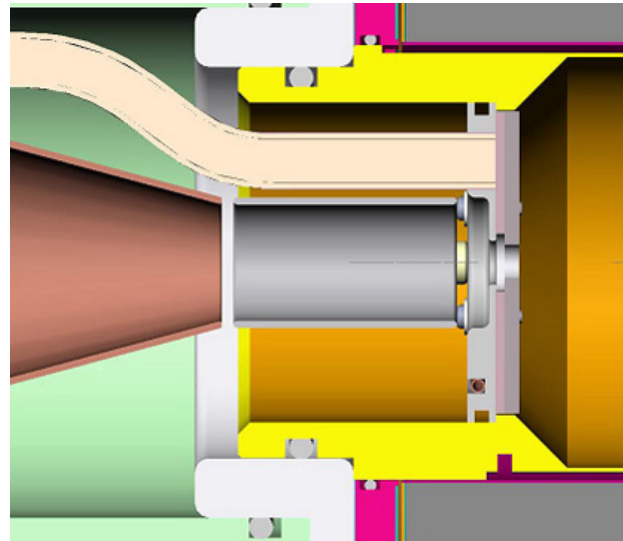

Figure 16. Detail cross section of the plasma endwall, second Einzel lens, ground shield, and WR-75 waveguide.
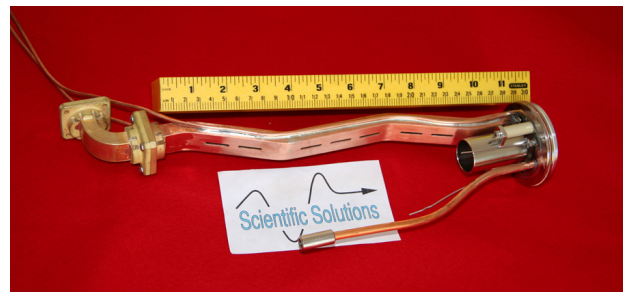

Figure 17. Plasma endwall assembly including the endwall, waveguide, gas feed tube, and second Einzel lens.

Figure 19 details the interior of the plasma endwall. The white ring is a boron-nitride disk that isolates the bias disk from the plasma chamber voltage. The rectangular cutout in the bias disk is for passing the rf energy from the waveguide into the plasma. The injected beam enters the plasma chamber through the hole in the center of the bias disk.

Figure 20 shows the first Einzel lens, mounting flange, and ground shield of the injector assembly. The ground shield protects the ion beam from the voltages on the components attached to the plasma chamber. Without this shield, the electric fields could disrupt the beam ions by steering and shearing the injected beam. The ground shield is electrically isolated from ground so that ion current impinging on the shield can be measured as a diagnostic tool. The mounting flange has the same pusher/puller alignment screws as the extractor assembly. Note that, like the extractor assembly, the injector system can be easily replaced.

Figure 18. Detail of the plasma endwall assembly. The blue arrow denotes the voltage connection to the bias disk on the inside of the endwall.

Figure 19. Close-up view of the inside of the plasma chamber endwall showing the bias disk and the white boron-nitride insulator.

Figure 21 shows the exterior of the injector vacuum cross. The white ring on top of the cross is a ceramic insulator that isolates the top flange from ground. All components attached to this top flange float at the voltage of the plasma chamber. The ion gauge is the blue box on the bottom flange. The turbomolecular vacuum pump is attached to the flange on the far side of the cross. The flange on the near side contains the high voltage feedthroughs for the Einzel lenses, a BNC connection to the ground shield, and a dial pressure gauge to indicate the status of the internal pressure when pumping down or venting the charge-breeder. The beam is injected through

a hole (yet to be cut) in the blank flange on the near end of the cross.

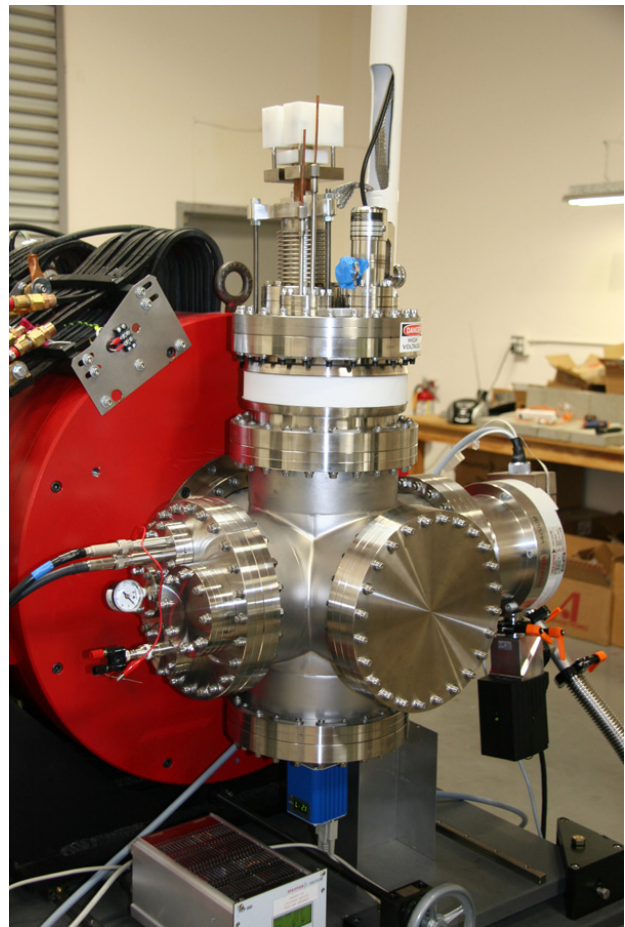**Figure 20.** Ground shield (left) and first Einzel lens (right) in the injection line.

Figure 21. View of the injector vacuum cross.

Charge Breeding

SUPPORT STAND

The support stand was designed to facilitate maintenance of the charge-breeder. Longitudinal space in accelerator beamlines is precious and removing downstream (or upstream) components to align the charge-breeder by sighting down the bore is undesirable. The support stand was designed to move transverse to the beamline on precision ball-bushing rail assemblies. Hence the charge-breeder can be removed from the beamline for maintenance without affecting the alignment of the charge-breeder or any other component in the beamline. Additionally, the precision nature of the rails ensures that the charge-breeder returns to precisely the same location as before. Hence the charge-breeder can be aligned by bore-sighting along a line parallel to the main beamline and moved into position on the rails without having to realign the system.

The support and alignment structure of the support stand is divided into two sections. The charge-breeder components are aligned on an aluminum tooling plate that serves as a base plate for this assembly. This base plate is "floating" on a separate set of adjustments. The components of the charge-breeder are aligned relative to each other on the base plate and then, once moved into position, the base plate is aligned relative to the axis of the beamline.

SUMMARY

Figure 22 is an overhead view of the charge-breeder from the injector end prior to shipping to Texas A&M University. The large red cylinders are the solenoid magnets. The electronic equipment rack is on the left and is connected to the high voltage platform on the charge-breeder through the white PVC tube. The water chiller for cooling the plasma tube is located just behind the equipment rack. The vacuum control and interlock chassis and the turbopump controllers are located on the temporary table just to the left of the charge-breeder. The rotary vane vacuum pumps are located on the floor just to the right of the charge-breeder. The vacuum pressure stabilized in the high 10^{-8} Torr range prior to disassembly and shipping. The charge-breeder was shipped to Texas A&M University and installed in the target cave at the Cyclotron Institute in late October 2007. Since that time, the baseline vacuum pressure has dropped into the 10^{-9} Torr range.
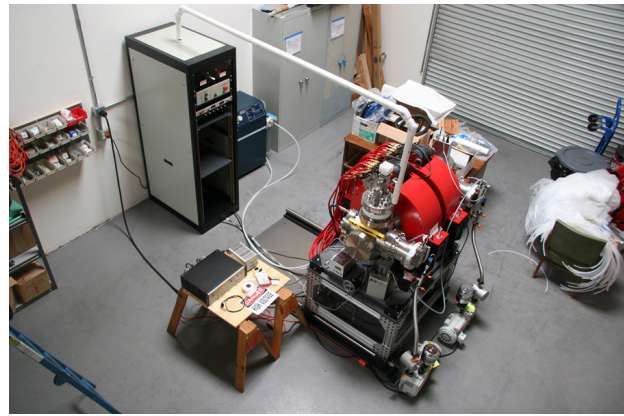

Figure 22. Overhead view of the charge-breeder prior to shipping to TAMU.

REFERENCES

[1] Z. Q. Xie and C. M. Lyneis, Rev. Sci. Instr. **66**(1995)4218

[2] M. Oyaizu, et. al., in Proc 15th International Workshop on ECR Ion Sources, ECRIS'02, June 12-14, 2002, University of Jyvaskyla, Finland

[3] M. Schlapp, et. al., in Proc. 1997 Particle Accelerator Conference, Vancouver BC, p. 2702

[4] J.-L. Bouly, et. al., in Proc. 16th Int. Conf. on Cyclotrons and Their Applications, Lansing MI, 2001, p. 228

[5] Recent data suggests that perhaps this minimum should be pushed even lower, perhaps as low as 0.5 B_{ECR}.

[6] While the relative magnitude of this peak field is subject to some discussion, there is universal agreement that the peak field at this end needs to be greater than the peak field at the extraction end.

[7] K. Halbach, Nucl. Instr. and Meth., **169** (1980), 1.

[8] Rexolite® is a thermoset, rigid, and translucent plastic produced by cross linking polystyrene with divinylbenzene. Rexolite has a combination of good physical and excellent electrical properties including low loss and stable dielectric constant and very low outgassing rate.